Impact of feed spacer filament spacing on mass transport and fouling propensities of RO membrane surfaces

Asim Saeed[1], Rupa Vuthaluru[1], Hari B.Vuthaluru[1]

[1]School of Chemical and Petroleum Engineering, Curtin University, Perth, Western Australia

Corresponding author's E-mail: h.vuthaluru@curtin.edu.au

Abstract

Material build-up on membrane surfaces is one of the vital challenges faced by Reverse Osmosis (RO) operations leading to many operational and maintenance issues. To date, several modelling studies dealt with flow behaviour and concentration patterns for cross-flow membrane operations. However, the relative fouling propensities of top and bottom membrane surfaces are never addressed in any study for narrow channels filled with ladder type spacers. In the present work, fluid flow patterns through different spacer configurations are visualized using ANSYS FLUENT by varying the dimensionless filament spacing, L (ratio of top or bottom filament spacing and channel height). Results clearly indicated that average shear stress values for the top membrane surface are always higher (3 to 8 times) than bottom membrane surface but yielded approximately similar average values of mass transfer coefficient for the two walls, for low to moderate filament spacings of $L \leq 3$ (SP22, and SP33) indicating similar fouling propensities of membrane surfaces. Further increase in filament spacing with $L \geq 4$ (SP44 and SP66), the average mass transfer coefficient for the top membrane indicated a sharp decline suggesting increased fouling propensity compared to bottom membrane which is not a desirable feature. Among the four spacer arrangements studied, SP44 (with L=4) was

found to be the optimal arrangement yielding moderate pressure drop with nearly equal/higher area weighted values of mass transfer coefficient for the two walls and would lead to lower and equal fouling tendencies for top and bottom membrane surfaces respectively.

KEYWORDS: CFD; RO Membrane; Spacers; Shear stress; Mass transfer coefficient; Build-up

INTRODUCTION

Material build-up on the membrane surfaces is considered to be one of the most important challenges during normal Reverse Osmosis (RO) operations. Several operational issues arising from scaling and fouling include: increased membrane resistance, decreased permeate flow rate, increased energy requirement and decreased membrane life. These issues have been addressed by several researchers, in a limited way, by proposing better pre-treatment processes (Baker et al. 1997; Wilf and Klinko 1998; Wilf and Schierach 2001; Bonnelye et al. 2004). However, there appears to be a need to change membrane or membrane secondary structures to alter the flow patterns associated with fluids within the membrane module. Schematic diagram of Spiral Wound Module (SWM), in partly unwounded state, has been presented earlier in one of our articles (Saeed et al. 2012). In case of SWM a number of flat membrane sheets are glued together, in pair arrangement, on three sides forming a pocket and a permeate spacer is introduced between the membranes pocket. The fourth open end of the membrane pocket is connected to a common permeate collector tube. The membrane

pockets are rolled around the tube with feed spacers between each pocket (Fritzmann et al. 2007; Peters 2010). As a result of the design, alternating feed and permeate channels are developed. Feed enters through one side of the module and is forced through the membrane. Retentate leaves the module from the opposite side of the feed inlet whereas permeate is collected in the common permeate tube.

The net spacer in the feed channel not only keeps the membrane layers apart, hence providing passage for the flow, but also significantly affects the flow and concentration patterns in the feed channel. They are responsible for the pressure drop and creation of limited flow zones (dead zones) and promote mixing between the fluid bulk and fluid elements adjacent to the membrane surface. In other words, they are intended to keep the membranes clean by enhancing mass transfer and disrupting the solute concentration boundary layer. In the past several experimental and theoretical studies were carried out to shed light on these phenomena and to optimize spacer configuration (G. Chatterjee and Belfort 1986; Fárková 1991; Zimmerer and Kottke 1996; Geraldes et al. 2002a; b; Geraldes et al. 2003; Koutsou et al. 2009; Picioreanu et al. 2009). So it is quite understandable that the presence of these spacers promotes directional changes in the flow which reduces membrane fouling and concentration polarization. Hence the efficiency of a membrane module depends heavily on the efficacy of the spacers to increase mass transport away from the membrane surface into the fluid bulk by increasing shear rate at the membrane surface (Da Costa et al. 1991).

Since spiral wound membranes have tightly wrapped structures which cannot be opened easily for chemical cleaning or cannot be back flushed by operating in reverse direction, the fouling control methods for SWM are limited to hydrodynamics, pre-treatment of the feed and operational controls (Fane et al. 2000). The fouling issues can be addressed to a large extent by varying the hydrodynamic conditions prevailing in spiral wound membrane. The feed spacers can be oriented to generate high cross flow velocities or secondary flow patterns which can develop higher scouring forces on the membrane surfaces to reduce fouling and concentration polarization. However, this approach will need higher pumping energy to compensate losses within the membrane module. Hence the feed spacers must be optimized to reduce the build-up on the membrane surface with moderate energy loss.

Our earlier work (Saeed et al. 2012) dealt with the impact of spacer filament orientation on hydrodynamics at fixed spacer mesh length. Although several modelling efforts dealt with the prediction of flow behaviour and concentration patterns for cross-flow membrane operations (Karode and Kumar 2001; Li et al. 2004; Ghidossi et al. 2006; Santos et al. 2006; Santos et al. 2007; Lau et al. 2009), the relative fouling propensities of top and bottom membrane surfaces are never addressed in any study. In view of this, an attempt has been made in the current study to predict the impact of fluid flow distribution on membrane wall shear stress and mass transfer coefficient by altering the filament mesh spacing utilising CFD tool. This detailed information from the numerical study is expected to provide insights into relative fouling propensities of two membrane surfaces for varying dimensionless spacer length.

GEOMETRIC PARAMETERS USED FOR SPACERS

In the present study channel height (h_{ch} - sum of the top and bottom filament diameters or thicknesses) as shown in Fig. 1(a) is used to non-dimensionalize spacer geometric parameters. Channel height is kept as 1mm for all the simulations in this work for the sake of convenience. The non-dimensionalized filament spacing for both top and bottom filaments are represented by the following relation:

$$L = \frac{l}{h_{ch}} = \frac{l_1}{h_{ch}} = L_1 = \frac{l_2}{h_{ch}} = L_2$$

In the above expression *l* refers to the mesh spacing whereas *L* represents the dimensionless filament spacing for filaments respectively. For the ease of understanding, the nomenclature followed to define a specific spacer configuration is represented by SPL_1L_2. Where SP is used as an abbreviation for Spacer and L_1 & L_2 are the dimensionless top and bottom filament spacing. Table 1 represents the four different cases studied in this work. In all the cases, the flow is defined in x-direction (see Fig. 1(a)) and the bottom and top filaments have same diameter and are oriented in transverse and axial directions to the main flow direction. Such type of spacer configuration is referred to as ladder type spacer arrangement.

Porosity And Hydraulic Diameter Of Spacer Filled Channel

Porosity of a spacer obstructed narrow channel can be defined by the following equation (Schock and Miquel 1987):

$$\varepsilon = 1 - \frac{V_{sp}}{V_T} \qquad (1)$$

In the above equation V_T represents the total volume of the channel, V_{sp} represents the spacer volume and ε represents porosity. The hydraulic diameter is defined by the following equation (Schock and Miquel 1987):

$$d_h = \frac{4\left(V_T - V_{sp}\right)}{S_{fc} + S_{sp}} \qquad (2)$$

In the above equation S_{fc} represents the wetted surface of the flat channel and S_{sp} represents wetted surface of the spacer and d_h represents the hydraulic diameter.

MODELLING APPROACH

Computational Domain And Boundary Conditions

The geometry of the spacer filled channel is of repeating nature and comprises of a large number of cells. There is a periodic variation in the cross section of such spacer filled channel. Fig. 2 shows the schematic of feed channel spacer and selected computational domain including 1-6 bottom filaments. Flow entering through one cell in the feed channel is identical to the flow entering the next adjacent cell in the span wise direction (y-direction in Fig. 1(a)). Moreover, in the flow direction there is translational periodicity i.e. along the flow direction (x-direction) the flow patterns repeat itself after periodic intervals. It has been shown in our previous study (Saeed et al. 2012) that entrance effects are eliminated after few filaments (3-4) and the flow becomes fully developed after few filaments in the flow direction. Translational periodic boundary conditions are implemented at the two faces perpendicular to the flow direction restricting the computational domain to only six bottom filaments and one top filament. In order to eliminate the exit effects sufficient exit length is provided to avoid the interference of the

outlet conditions with the recirculation regions after the last bottom filament. So the cell between the last two filaments will be a true representative of the flow and concentration patterns generated in a SWM. The boundary conditions used for the model are discussed below:

- The two opposite vertical faces perpendicular to the flow direction (x- direction) are defined as mass flow inlet and pressure outlet. Mass flow rate is specified in flow direction (x-direction) and varied to obtain the desired hydraulic Reynolds number (Re_h). The solute mass fraction at the inlet of the computational domain is set to zero.
- The working fluid is assumed to be a binary mixture of water and monovalent salt, such as sodium chloride having a mass diffusivity (D) of 1.54×10^{-9} m^2/s (Capobianchi et al. 1998). Working fluid is further assumed to be isothermal and incompressible and having constant density (998.2 Kg/m^3), viscosity (0.001 Kg/(m.s)) and solute diffusivity (1.54×10^{-9} m^2/s).
- Translational periodic boundary conditions are defined for the two vertical surfaces parallel to top filaments and the filament surfaces are defined as walls.
- Both top and bottom membrane surfaces are assumed to be impermeable walls and no slip conditions are assigned to them.
- Constant higher value of solute mass fraction is defined at both the membrane walls. In all the simulations the solute mass fraction at the walls were assigned a value of 1, whereas the mass fraction of the solute is defined as zero at the inlet of the computational domain. Since cross flow filtration processes tend to recover only 10 to 15 % of the feed as product and also have large surface area, therefore large surface area coupled with low recovery rates yields very low permeation velocities compared to feed

velocity, hence the assumption of impermeable walls for both top and bottom membrane surfaces of the computational domain is justified (Fimbres-Weihs and Wiley 2010). Although there will be an increase in the solute mass fraction at the membrane surfaces in the flow direction as a result of separation process but due to low permeation rate through the membrane surfaces the variation of local concentration on the membrane walls along the flow direction is negligible and hence top and bottom membrane walls are set to be at higher fixed values of concentration than at the inlet (Fimbres-Weihs and Wiley 2010). It has also been established by previous researchers that the choice of mass fraction values at the membrane surface and at the inlet does not have impact on the mass transfer results obtained, provided they are not set approximately equal to avoid numerical round-off errors (Fimbres-Weihs and Wiley 2010).

Literature review to date reveals that for the same type of spacers, spacer-filled flat channels and SWM channels show similar flow characteristics (Schock and Miquel 1987; Ranade and Kumar 2006a). Ranade and Kumar (Ranade and Kumar 2006b) in another study concluded that the transition from laminar to turbulent flow regime for most of the spacer-filled channels occurs at Reynolds numbers of 300-400 (based on hydraulic diameter) as reported for packed beds. In the present study we have used laminar flow, steady-state model as hydraulic Reynolds number (Re_h) was kept 100 for all the cases. In most of the real life cases flow through spacer filled modules do fall in the Reynolds number category where the flow is steady and laminar (Fimbres-Weihs and Wiley 2007) and justifies our choice of steady-state and laminar flow regime. In the present study, steady state and laminar flow conditions are therefore employed to investigate the impact

of dimensionless filament mesh spacing on wall shear stress and mass transfer coefficient for the two membrane walls which indirectly dictates the relative fouling propensities of two membrane surfaces during membrane operations.

Hydraulic Reynolds number is used in the present study to compare results of different spacer arrangements and it is defined by the following equation (Schock and Miquel 1987):

$$Re_h = \frac{d_h u_{eff}}{\boldsymbol{v}} \qquad (3)$$

In the above equation u_{eff}, d_h and $\boldsymbol{v}$ represents the effective velocity (or average) in the computational domain, hydraulic diameter of the channel and kinematic viscosity respectively. The effective velocity is calculated at a particular hydraulic Reynolds number and then used to calculate mass flow rate at the inlet of computational domain.

For spacer filled narrow channels, Sherwood number (*Sh*) using the hydraulic diameter of the channel is defined by the following equation:

$$Sh = \frac{k_{av} d_h}{D} \qquad (4)$$

In the above relation *D* and k_{av} represents the mass diffusivity and average mass transfer coefficient for the two membrane surfaces.

Furthermore, to validate the present model, friction factor values for the spacers calculated by using equation 5 are compared with numerical and experimental results of

Geraldes et al. (Geraldes et al. 2002b). Following equation is employed for the calculation of friction factor (Geraldes et al. 2002b):

$$f = \frac{\Delta P}{L_c} \frac{h_{ch}}{\rho u_{eff}^2} \tag{5}$$

In the above expressions, L_c and ΔP are the channel length and pressure drop over the channel respectively, whereas ρ is the density.

Da Costa et al. (Da Costa et al. 1994) in their research work showed that Grober equation predicts Sherwood number for spacer filled narrow channels within $\pm$30% error. For the spacers, having filament oriented along axial and transverse direction to the fluid flow, Grober equation is presented as (Da Costa et al. 1994):

$$Sh_{Grober} = 0.664\, Re_h^{0.5}\, Sc^{0.33} \left[\frac{d_h}{l}\right]^{0.5} \tag{6}$$

For the validation of the current model, computationally determined Sherwood number (obtained from equation 4) for different spacer arrangements are also compared with those obtained from equation 6. In the above equation Sc is Schmidt number defined as the ratio of momentum and mass diffusivity $\left(Sc = \upsilon / D\right)$ and l represents the filament spacing.

Considering the degree of accuracy of the results needed, computational time required and available computational resources a grid size of 716,880 was chosen as an adequate grid size for SP22. Similarly adequate grid sizes for different spacer arrangement were

determined to ensure the solution is grid independent. For instance approximately 1.6 and 6 Million cells were found to be sufficient for spacers SP33 and SP66 respectively.

Governing Equations, Solution Methods And Convergence Criteria

Continuity, three momentum equations (x, y and z momentum) and concentration equations are the five governing equations (Navier-Stokes equations) which are represented below for steady, laminar and incompressible flow in three-dimensional form (Bird et al. 1960):

$$\frac{\partial u}{\partial x}+\frac{\partial v}{\partial y}+\frac{\partial w}{\partial z}=0 \tag{7}$$

$$u\frac{\partial u}{\partial x}+v\frac{\partial u}{\partial y}+w\frac{\partial u}{\partial z}=-\frac{1}{\rho}\frac{\partial P}{\partial x}+\upsilon\left[\frac{\partial^2 u}{\partial x^2}+\frac{\partial^2 u}{\partial y^2}+\frac{\partial^2 u}{\partial z^2}\right] \tag{8}$$

$$u\frac{\partial v}{\partial x}+v\frac{\partial v}{\partial y}+w\frac{\partial v}{\partial z}=-\frac{1}{\rho}\frac{\partial P}{\partial y}+\upsilon\left[\frac{\partial^2 v}{\partial x^2}+\frac{\partial^2 v}{\partial y^2}+\frac{\partial^2 v}{\partial z^2}\right] \tag{9}$$

$$u\frac{\partial w}{\partial x}+v\frac{\partial w}{\partial y}+w\frac{\partial w}{\partial z}=-\frac{1}{\rho}\frac{\partial P}{\partial z}+\upsilon\left[\frac{\partial^2 w}{\partial x^2}+\frac{\partial^2 w}{\partial y^2}+\frac{\partial^2 w}{\partial z^2}\right] \tag{10}$$

$$u\frac{\partial Y}{\partial x}+v\frac{\partial Y}{\partial y}+w\frac{\partial Y}{\partial z}=D\left[\frac{\partial^2 Y}{\partial x^2}+\frac{\partial^2 Y}{\partial y^2}+\frac{\partial^2 Y}{\partial z^2}\right] \tag{11}$$

ANSYS FLUENT is used to solve the governing equations and pressure based segregated solver is employed for the solution. QUICK (Quadratic Upstream Interpolation for Convective Kinetics) scheme is used for discretising momentum equations, whereas SIMPLEC (Semi-Implicit Method for Pressure linked Equations, Consistent) algorithm is

used for pressure velocity coupling (Versteeg and Malalasekera 2007; Fluent 2009). However, for the discretization of concentration equation power law scheme is employed.

The convergence criterion for the scaled residuals of continuity, x, y and z components of velocity and solute mass fraction were set to 1e-06. Additional confirmation for reliability of the converged results was obtained by observing the stable values of velocity and solute mass fraction at different monitoring points defined in the computational domain. Fig. 1(b) represents the monitoring points (MP1 & MP2) selected within the specific area of interest in the computational domain. Fig. 1 (c&d) represents the corresponding velocities and solute mass fractions at MP1 and MP2 respectively versus the number of iterations. It was ensured that the numerical values of velocity magnitude and mass fraction are also stabilized at defined monitoring points in the computational domain in the area of interest (between the last two bottom filaments in the flow direction).

Incorporation Of Mass Transfer Coefficient Into The Model

In case of spacer filled narrow channels having impermeable membrane walls, the local and average mass transfer coefficients can be defined respectively by the following equations (Kang and Chang 1982; Fletcher et al. 1985):

$$k_l = \frac{D}{Y_w - Y_b}\left[\frac{\partial Y}{\partial z}\right]_w \qquad (9)$$

$$k_{av} = \frac{1}{A}\sum_{i=1}^{n} k_l A_i \qquad (10)$$

In the above equations k_l, k_{av} are the local and average mass transfer coefficients. The terms Y_w, Y_b and $\left[\frac{\partial Y}{\partial z}\right]_w$ represents mass fraction of the solute at the membrane wall, mass fraction of solute in the bulk and gradient of mass fraction at the membrane wall respectively. The terms A and A_l represents the membrane surface area and face area of any computational cell respectively. The above mentioned pair of equations is used often by researchers, simulating mass transport of solute for impermeable membrane walls scenarios, for CFD simulations (Kang and Chang 1982; Fletcher et al. 1985). Mass transport equation is incorporated in our numerical model by means of a user defined function.

Selected Domain Representative Of SWM Module

As described earlier the computational domain for all spacer arrangements considered in this study consists of six bottom filaments and one top filament to provide sufficient entrance region to make sure that the flow and the concentration patterns are stabilized within the computational domain before the exit (Fig. 1(a)). Sufficient exit length is incorporated in the computational domain to eliminate any exit effects that may impact the upstream flow and concentration patterns.

In order to investigate which part of the flow domain is true representative of the whole SWM, top and bottom wall shear stresses and mass transfer coefficients are plotted along flow direction on bottom and top membrane walls (along lines A and B respectively) as shown in Fig. 2(a). Variation in local values of mass transfer coefficient and shear stress

at bottom and top membrane walls along lines A & B are shown in Fig. 2(b & c). It can be seen from the Fig that the shear stress variation along the flow direction is not identical in the entrance region (first two filaments). However, at the third and fourth bottom filament those variations appear to become identical ensuring that the flow has been fully developed and periodic at the third bottom filament.

The plot for mass transfer coefficient for the two walls starts with a very high value for mass transfer coefficient at the inlet due to larger concentration difference between the entering fluid and membrane walls (Fig. 2 (b &c)). For the first two filaments the local variations for mass transfer coefficient is also not identical but somewhere near the third bottom filament the local values for mass transfer coefficient tend to get stabilised and repeat in a periodic manner along the flow direction. The trends showing the local variation of mass transfer coefficient and wall shear stress along the flow direction for both the walls are found similar to earlier two dimensional (Cao et al. 2001; Song and Ma 2005; Ma and Song 2006) and three dimensional CFD studies (Shakaib et al. 2009) reported in the literature.

In real life, there are thousands of filaments present at the feed side channel of a spiral wound membrane module and the first two filaments of the selected computational domain cannot be the true representation for an entire real life membrane module (Fig. 1(a)). Similarly, the region between the last bottom filament and the exit do not represent the actual mass transfer and shear stress variations in the major portion of a spiral wound module. However, in the region between 5^{th} and 6^{th} bottom filament the flow and

concentration patterns are fully developed and are identical to the patterns developed in the region between 4th and 5th bottom filament. Hence, it can be concluded that the region between the 5th and 6th bottom filament may be selected as true representative of the flow and concentration patterns prevailing in the major portion of a real life spiral wound membrane module (see Fig. 1(b)).

Selection of the region between the 5th and 6th bottom filament is further strengthened by the comparisons of contours of mass transfer coefficient and wall shear stress for the region between 4th and 5th and 5th and 6th bottom filament. In Fig. 3 mass transfer coefficient and wall shear stress contours between the selected region (between 5th and 6th bottom filament) and adjacent region (between 4th and 5th bottom filament) are presented for only two spacer arrangements considered in this work. These contours for the stated regions are also identical for all the spacers considered in the work.

Based on the above discussion, it can be inferred that the region between the last two filaments (in the flow direction i.e. between 5th and 6th filament) may be taken as a true representative of the flow and concentration patterns generated in major portion of a spiral wound membrane module. All the reported values and comparisons are made in the current work are based on numerical values and trends from the selected portion of the computational domain.

RESULTS AND DISCUSSION

The impact of altering filament mesh spacing on wall shear stress, pressure drop and relative fouling propensities of top and bottom membrane surfaces (in terms of area weighted average mass transfer coefficient values) is investigated in the present work and the results are discussed for different spacer configurations.

The fluid flow patterns are quite complex in the vicinity of the bottom membrane surface for the ladder type spacer arrangement. This is because the bulk of the fluid, in the vicinity of the top membrane wall, follows the main flow direction and hence for the major portion of top membrane wall shear stress and local mass transfer coefficient values follow the same trend i.e. they increase or decrease simultaneously at different locations with the exception of very small regions where the flow separates and reattaches from and to the top filament. However, there are strong three dimensional effects seen in the vicinity of the bottom membrane wall due to flow reattachment and separation phenomena covering a larger portion of the bottom membrane.

Fig. 4 presents the velocity vectors at a plane very close to top and bottom membranes respectively. The regions of flow separation and reattachment are also indicated in the figure. As a result of flow separation and reattachment, the local wall shear stress and mass transfer coefficient do not follow same trend as in case of top membrane wall as shown in Fig. 5. Fig. 5 (a) represents the contours of velocity magnitude overlaid by velocity vectors (fixed length) at a vertical plane (y = 0mm) and Fig. 5 (b &c) represents the local distribution of wall shear stress and mass transfer coefficient at the bottom and top wall respectively along the normal flow direction at y = 0mm. There is a reduction in

cross sectional flow area due to the presence of bottom (transverse) filament and the fluid tends to accelerate when crossing over the bottom filament. This phenomenon induces a nozzle like effect which results in higher local wall shear stress and mass transfer coefficient values at the top membrane wall directly above the bottom filaments which is evident in Fig. 5 (c). Fluid in the upper portion of the feed channel after being accelerated over the bottom filament tends to undergo deceleration due to higher available flow area (to justify continuity) and thus yield lower local values of shear stress and mass transfer coefficient at the top wall till it gets accelerated again just above the downstream bottom filament.

In the vicinity of the bottom membrane, fluid tends to reattach with the bottom membrane surface in the middle of the two consecutive bottom filaments and further undergoes flow reversal and recirculation. This recirculation induces a scouring action on major portion of the bottom membrane and hence results in higher values of mass transfer coefficient for major part of the bottom membrane. However, there are also some stagnant fluid regions very close to the bottom filaments in the vicinity of the bottom membrane which results in lower values of local wall shear stress and mass transfer coefficient.

There are three regions where the wall shear stress shows almost zero values but the mass transfer coefficient values are higher. Out of the three regions, two regions represent the area just after and just before the transverse upstream and downstream filament. It can be seen from Fig. 5 (b) that the fluid in those areas tends to separate from the bottom filaments (labelled as “Separation Region” in Fig. 5 (b)) and as a result associated

directional changes enhances the local mass transfer coefficient. Moreover the fluid velocity in those areas is very small which leads to minimum wall shear stress in those regions.

The third region where the mass transfer coefficient curve shows local peak despite minimum value of local wall shear stress resides somewhere in the middle of the two bottom transverse filaments. It can be seen from Fig. 5 (a), that particular region corresponds to the zone where the fluid reattaches itself to the bottom membrane surface and undergoes strong directional changes leading to enhanced local mass transfer coefficient despite very low local velocity and wall shear stress. It can be concluded from Fig. 5 (b) that lower local value of wall shear stress does not necessarily mean lower local value for mass transfer coefficient.

Fig. 6 represents the velocity vectors on a plane near the membrane surfaces overlayed by the mass transfer coefficient contours for different spacer arrangements considered in the current study (see Table 1). It is quite evident that spacers having $L \leq 3$ (SP22 and SP33) show only flow reversal and when it is increased to 4 and above (SP44 and SP66) both flow reattachment and reversal regions are seen. There are four important regions each on the top and bottom membrane surfaces in terms of variation in mass transfer coefficient and are marked as A-D & E-H for top and bottom membranes respectively for SP44 in Fig. 6. The fluid tends to shift away from the top axial filament in the region A and leads to lower values of mass transfer coefficient. The fluid while proceeding in the normal flow direction tends to reattach to the top filament in the region where the top filament

crosses over the bottom filament and yields higher local values for mass transfer coefficient in region B. Mass transfer coefficient is also observed to be higher in the region C when high velocity fluid flows over the bottom filament and when the flow detaches from the top membrane in region D the mass transfer coefficient drops down. On the bottom membrane surface, mass transfer coefficient exhibits higher local values in region E where the fluid reattaches to the surface. It is interesting to notice that this region is absent for SP22 and SP33 because the fluid does not reattach to the bottom membrane surface and undergoes recirculation after hitting the downstream bottom filament. In region F just after the upstream filament a stagnant fluid zone is created which leads to lower values of mass transfer coefficient. The size of this stagnant region reduces with the increase in the filament spacing as seen in Fig. 6 and is highly desirable for efficient process. Low values of mass transfer coefficient are observed just below the top filament on the bottom membrane surface in region G. In the vicinity of the downstream bottom filament (region H) fluid undergoes strong directional changes (in Y direction) due to the presence of bottom filament and results in higher value for the mass transfer coefficient. It can be seen from the Fig. 6 that the relative size of the zone H and local values of mass transfer coefficient in that zone reduces when the filament spacing is increased.

Furthermore, it has been observed that the dimensionless bottom filament mesh length (L_2) has an important role to define the flow patterns near the bottom membrane surface. Upon investigating different spacers it is concluded that when L_2 is up to 3, the flow after colliding the downstream transverse bottom filament reverses its direction and region of

reattachment is absent for those spacers. However, flow reattachment region appears for the spacers having $L_2 > 3$ which is line with our previous study (Saeed et al. 2012) and other modelling studies (Shakaib et al. 2007; 2009) involving flow through spacer obstructed narrow feed channels when the top and bottom feed channel side spacers are oriented in axial and transverse direction to the main flow.

The impact of altering filament spacing on area weighted mass transfer coefficient and shear stress on the two walls along with pressure drop for various spacers studied are presented in Fig. 7 (a &b) and the results are summarised in Table 2. It can be seen from Table 2 that for narrow channels obstructed by ladder type spacers, linear pressure drop declines with an increase in filament mesh spacing. Shear stress values are always higher for the top membrane surface and the ratio of the two wall shear stresses tend to decline with an increase in the filament mesh spacing. However, the ratio of top and bottom mass transfer coefficients shows a different trend. The ratio is approximately unity for low to moderate filament spacing and declines sharply for the spacers having higher filament spacing (see Table 2).

It can be observed from Fig. 7 (b) that although pressure drop for SP66 is lower compared to SP44, but the difference in mass transfer coefficient for the two membrane walls is significant indicating a varying fouling tendency for the two membrane surfaces and certainly not desirable for membrane operations. It can be seen that the top and bottom wall shear stress differ significantly for each type of spacer arrangement (Fig.11 (a)). However, the values for mass transfer coefficient are almost the same for the spacers

having low to moderate dimensionless filament spacing (SP22, SP33 and SP44). With a further increase in filament mesh spacing (SP66) although the values for top and bottom wall shear stresses tend to get closer (see Table 2) but the resulting impact on the mass transfer coefficient is not desirable, as this could lead to significant drop in top wall mass transfer coefficient resulting in quick fouling of the top membrane wall.

VALIDATION OF CURRENT MODEL

For validation of the current model used in this work, results for some spacer configurations are compared with some previous experimental and numerical studies for selected dimensionless parameters such as friction factor (f) and Sherwood number (Sh) which reflects the flow and mass transport phenomena through membrane systems. The details of model validation are discussed below.

Friction Factor (F)

Friction factor values calculated for SP22, SP44 and SP66 by equation 5 are compared with experimental and numerical values presented by Geraldes et al. (Geraldes et al. 2002b) for spacer configuration termed as S1, S2 and S3 respectively in their work having transverse dimensionless filament spacings of 1.9, 3.8 and 5.7. The comparison shown in Fig. 8(a) reveals that the friction factor values obtained from the present numerical study is in excellent agreement (within 4% deviation) with those obtained experimentally and numerically by Geraldes et al. (Geraldes et al. 2002b).

Sherwood Number (Sh)

To compare Sherwood number obtained from the present numerical study with experimental work of Li et al. (Li et al. 2004), simulations were carried out for few spacers at Schmidt number of 1350 (as used by Li et al. (Li et al. 2004)). Sherwood numbers obtained for SP22, SP33 and SP44 spacer configurations are compared with those studied by Li et al. (Li et al. 2004) having dimensionless filament spacings of L= 2.2, 2.8 and 4 respectively. Comparisons also included the values obtained by using Grober equation defined by Da Costa et al. (Da Costa et al. 1994) for ladder type spacer arrangement. Fig. 8(b) presents the comparison of the Sherwood number obtained by the present study with experimental work of Li et al. (Li et al. 2004) and Grober equation for ladder type spacers. It can be seen from Figure that Sherwood number obtained from the current work for different spacer arrangements is in fair accordance with previous experimental and numerical studies. It should be noted from the comparisons that Grober equation suggested by De Costa el al. (Da Costa et al. 1994) for ladder type spacers presents a relatively higher value for SP22 (approximately 30% higher). This is attributed due to fact that Grober equation presented by De Costa et al. (Da Costa et al. 1994) for ladder type space arrangement predicts the mass transfer rate with $\pm$ 30% error as reported in their manuscript.

CONCLUSIONS

Present study dealt with flow patterns generated within feed channel of spacer obstructed modules and their resulting impact on shear stress, mass transfer coefficient and relative fouling propensity of the two membrane surfaces, by altering the filament mesh spacing of ladder type feed spacers. Flow visualizations carried out in this study clearly indicate

that the fluid flow patterns, mass transfer coefficient and wall shear stress distribution along with the pressure drop are largely dependent on the filament mesh spacing.

Although the wall shear stress at the top membrane surface is always higher (3 to 8 times for the spacer arrangements considered in the study) than that for bottom wall, but interestingly the mass transfer coefficient values for the two walls are not significantly different for the ladder type spacer arrangement having low to moderate filament spacing (SP22, SP33 and SP44). However, when the filament spacing is further increased (SP66), there is a sharp decline in the pressure drop but the area weighted mass transfer coefficient for the top membrane wall showed a sharp reduction compared to the bottom membrane wall suggesting high fouling propensity of the top membrane wall which is not a desirable feature in membrane operations. Among the four cases studied, SP44 with dimensionless filament spacing of 4 is found to be the best spacer arrangement yielding moderate pressure drop with nearly equal and higher area weighted values of mass transfer coefficient for the two walls and would lead to lower and equal fouling tendency for top and bottom membrane surfaces. The results emanated out of the current study are considered to be of significant value and could potentially lead to the development of efficient membrane modules with optimum spacer arrangements for RO operations.

NOMENCLATURE

A membrane surface area (m^2)

A_i face area of computational cell (m^2)

D mass diffusivity (m^2/s)

d_h hydraulic diameter (m)

h_{ch} channel height (m)

k_{av} average mass transfer coefficient (m/s)

$k_{av,top}$ & $k_{av,bot}$ average mass transfer coefficient for top and bottom wall (m/s)

k_l local mass transfer coefficient (m/s)

L_1 & L_2 dimensionless top and bottom filament spacing

L_c channel length (m)

l_1& l_2 top and bottom filament spacing (m)

P pressure (Pa)

ΔP pressure drop (Pa)

Re_h hydraulic Reynolds number

S_{fc} wetted surface of flat channel (m^2)

S_{sp} wetted surface of spacer (m^2)

u_{eff} effective velocity (m/s)

V_{sp} spacer volume (m^3)

V_T total channel volume (m^3)

Y_w, Y_b solute mass fraction at wall and in the bulk

$\left[\frac{\partial Y}{\partial z}\right]_w$ mass fraction gradient at membrane wall (1/m)

u x-component of velocity (m/s)

v y-component of velocity (m/s)

w z-component of velocity (m/s)

x x-coordinate (m)

y y-coordinate (m)

z z-coordinate (m)

τ_{top} & τ_{bot} top and bottom membrane wall shear stress (N/m^2)

υ kinematic viscosity (m^2/s)

ε porosity or voidage

ρ density (kg/m^3)

REFERENCES

Baker, J. S., et al. (1997). Antiscale magnetic pretreatment of reverse osmosis feedwater. *Desalination* **110**(1–2), 151-165.

Bird, R. B., et al. (1960). *Transport Phenomena*, John Wiley & Sons, New York

Bonnelye, V., et al. (2004). Reverse osmosis on open intake seawater: pre-treatment strategy. *Desalination* **167(0)**: 191-200.

Cao, Z., et al. (2001). CFD simulations of net-type turbulence promoters in a narrow channel. *J. Membr. Sci.* **185(2)**: 157-176.

Capobianchi, M., et al. (1998). A new technique for measuring the Fickian diffusion coefficient in binary liquid solutions. *Exp. Therm. Fluid. Sci.* **18(1)**: 33-47.

Da Costa, A., et al. (1994). Spacer characterization and pressure drop modelling in spacer-filled channels for ultrafiltration. *J. Membr. Sci.* **87(1-2)**: 79-98.

Da Costa, A. R., et al. (1991). Optimal channel spacer design for ultrafiltration. *J. Membr. Sci.* **62(3)**: 275-291.

Fane, A., et al. (2000). Membrane fouling and its control in environmental applications. *Water Sci. Technol.*: 303-308.

Fárková, J. (1991). The pressure drop in membrane module with spacers. *J. Membr. Sci.* **64(1-2)**: 103-111.

Fimbres-Weihs, G. and D. Wiley (2010). Review of 3D CFD modeling of flow and mass transfer in narrow spacer-filled channels in membrane modules. *Chem. Eng. Process.: Process Intensification* **49(7)**: 759-781.

Fimbres-Weihs, G. A. and D. E. Wiley (2007). Numerical study of mass transfer in three-dimensional spacer-filled narrow channels with steady flow. *J. Membr. Sci.* **306(1-2)**: 228-243.

Fletcher, D., et al. (1985). Heat and mass transfer computations for laminar flow in an axisymmetric sudden expansion. *Comput. Fluids* **13(2)**: 207-221.

Fluent (2009). *ANSYS Fluent Documentation. V***ersion 12.0/12.1**

Fritzmann, C., et al. (2007). State-of-the-art of reverse osmosis desalination. *Desalination* **216(1-3)**: 1-76.

G. Chatterjee, S. and G. Belfort (1986). Fluid flow in an idealized spiral wound membrane module. *J. Membr. Sci.* **28(2)**: 191-208.

Geraldes, V., et al. (2002a). The effect of the ladder-type spacers configuration in NF spiral-wound modules on the concentration boundary layers disruption. *Desalination* **146(1-3)**: 187-194.

Geraldes, V., et al. (2002b). Flow management in nanofiltration spiral wound modules with ladder-type spacers. *J. Membr. Sci.* **203(1-2)**: 87-102.

Geraldes, V., et al. (2003). Hydrodynamics and concentration polarization in NF/RO spiral-wound modules with ladder-type spacers. *Desalination* **157(1-3)**: 395-402.

Ghidossi, R., et al. (2006). Computational fluid dynamics applied to membranes: State of the art and opportunities. *Chem. Eng. Process.* **45(6)**: 437-454.

Kang, I. S. and H. N. Chang (1982). The effect of turbulence promoters on mass transfer—numerical analysis and flow visualization. *Int. J. Heat Mass Transfer* **25(8)**: 1167-1181.

Karode, S. K. and A. Kumar (2001). Flow visualization through spacer filled channels by computational fluid dynamics I.: Pressure drop and shear rate calculations for flat sheet geometry. *J. Membr. Sci.* **193(1)**: 69-84.

Koutsou, C., et al. (2009). A numerical and experimental study of mass transfer in spacer-filled channels: effects of spacer geometrical characteristics and Schmidt number. *J. Membr. Sci.* **326(1)**: 234-251.

Lau, K. K., et al. (2009). Feed spacer mesh angle: 3D modeling, simulation and optimization based on unsteady hydrodynamic in spiral wound membrane channel. *J. Membr. Sci.* **343(1-2)**: 16-33.

Li, F., et al. (2004). Experimental validation of CFD mass transfer simulations in flat channels with non-woven net spacers. *J. Membr. Sci.* **232(1-2)**: 19-30.

Ma, S. and L. Song (2006). Numerical study on permeate flux enhancement by spacers in a crossflow reverse osmosis channel. *J. Membr. Sci.* **284(1-2)**: 102-109.

Peters, T. (2010). Membrane Technology for Water Treatment. *Chem. Eng. Technol.* **33(8)**: 1233-1240.

Picioreanu, C., et al. (2009). Three-dimensional modeling of biofouling and fluid dynamics in feed spacer channels of membrane devices. *J. Membr. Sci.* **345(1-2)**: 340-354.

Ranade, V. V. and A. Kumar (2006a). Comparison of flow structures in spacer-filled flat and annular channels. *Desalination* **191(1-3)**: 236-244.

Ranade, V. V. and A. Kumar (2006b). Fluid dynamics of spacer filled rectangular and curvilinear channels. *J. Membr. Sci.* **271(1-2)**: 1-15.

Saeed, A., et al. (2012). Effect of feed spacer arrangement on flow dynamics through spacer filled membranes. *Desalination* **285(0)**: 163-169.

Santos, J., et al. (2007). Investigation of flow patterns and mass transfer in membrane module channels filled with flow-aligned spacers using computational fluid dynamics (CFD). *J. Membr. Sci.* **305(1-2)**: 103-117.

Santos, J. L. C., et al. (2006). Modelling of flow and concentration patterns in spiral wound membrane modules with ladder-type spacers. *Desalination* **200(1-3)**: 395-396.

Schock, G. and A. Miquel (1987). Mass transfer and pressure loss in spiral wound modules. *Desalination* **64**: 339-352.

Shakaib, M., et al. (2007). Study on the effects of spacer geometry in membrane feed channels using three-dimensional computational flow modeling. *J. Membr. Sci.* **297(1-2)**: 74-89.

Shakaib, M., et al. (2009). CFD modeling for flow and mass transfer in spacer-obstructed membrane feed channels. *J. Membr. Sci.* **326(2)**: 270-284.

Song, L. and S. Ma (2005). Numerical studies of the impact of spacer geometry on concentration polarization in spiral wound membrane modules. *Ind. Eng. Chem. Res.* **44(20)**: 7638-7645.

Versteeg, H. K. and W. Malalasekera (2007). *An introduction to computational fluid dynamics: the finite volume method*, Prentice Hall

Wilf, M. and K. Klinko (1998). Effective new pretreatment for seawater reverse osmosis systems. *Desalination* **117(1–3)**: 323-331.

Wilf, M. and M. K. Schierach (2001). Improved performance and cost reduction of RO seawater systems using UF pretreatment. *Desalination* **135(1–3)**: 61-68.

Zimmerer, C. C. and V. Kottke (1996). Effects of spacer geometry on pressure drop, mass transfer, mixing behavior, and residence time distribution. *Desalination* **104(1-2)**: 129-134.

ACCEPTED MANUSCRIPT

Table 1 Spacer arrangements considered for the current study

Spacer configuration	SP22	SP33	SP44	SP66
L_1	2	3	4	6
L_2	2	3	4	6

Table 2 Summary of results for various spacer configurations at Re_h=100

Configuration	τ_{top}	τ_{bot}	$k_{av,top}$ x10^5	$k_{av,bot}$ x10^5	$\Delta P / L_c$	τ_{top} / τ_{bot}	$k_{av,top} / k_{av,bot}$
	N/m^2	N/m^2	m/s	m/s	Pa/m	-	-
SP22	1.77	0.22	3.94	4.46	9344	8.04	0.88
SP33	1.18	0.19	3.78	3.69	5285	6.21	1.02
SP44	0.86	0.14	3.59	3.69	3536	6.14	0.97
SP66	0.60	0.21	2.52	3.58	2131	2.86	0.70

Figure 1 (a) Schematic of feed channel spacer and selected computational domain (1-6 refer to bottom filaments) (b) Monitoring points (MP1 & MP2) in selected part of computational domain (between 5th & 6th bottom filaments) (C) Solute mass fraction vs iterations at MP2 (D) velocity magnitude vs iterations at MP1.

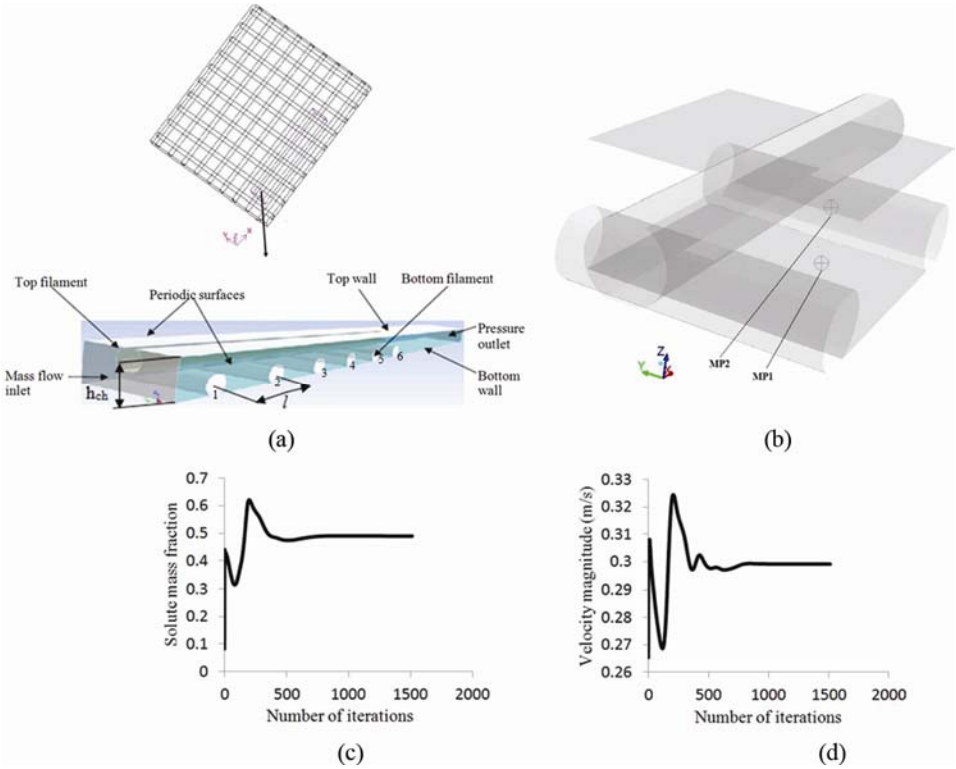

Figure 2 (a) Total computational domain with lines A & B on bottom and top walls. Shear stress and Mass transfer coefficient distribution on (b) bottom and (c) top walls for SP44 at Reh=100 (Vertical lines indicate the centre line of bottom filaments).

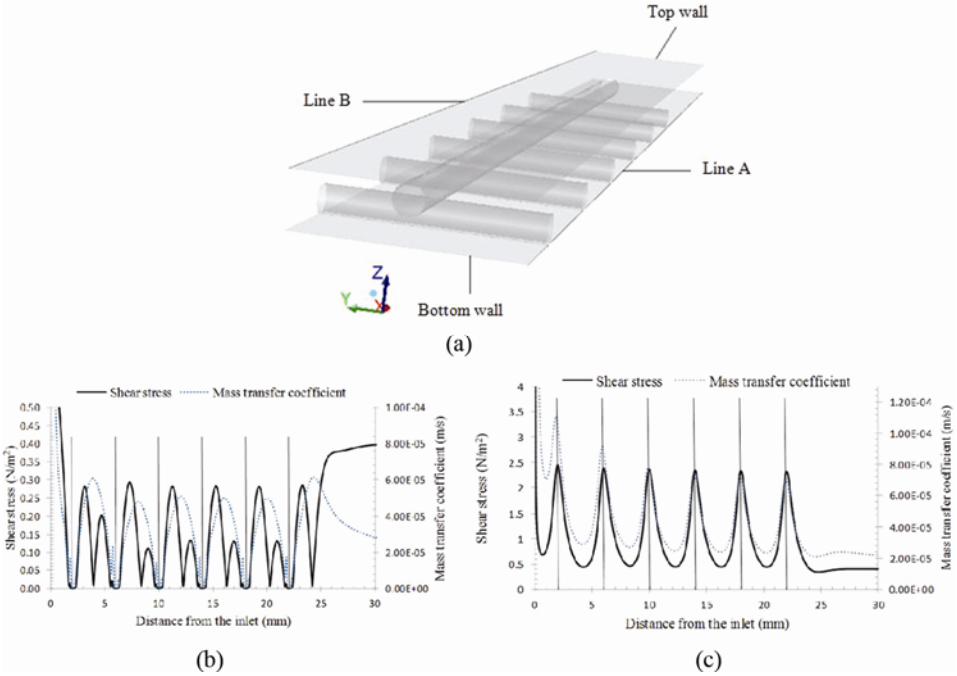

Figure 3 Contours of (a) wall shear stress and (b) mass transfer coefficient for different spacers at Re_h=100 between the selected and adjacent region of the computational domain.

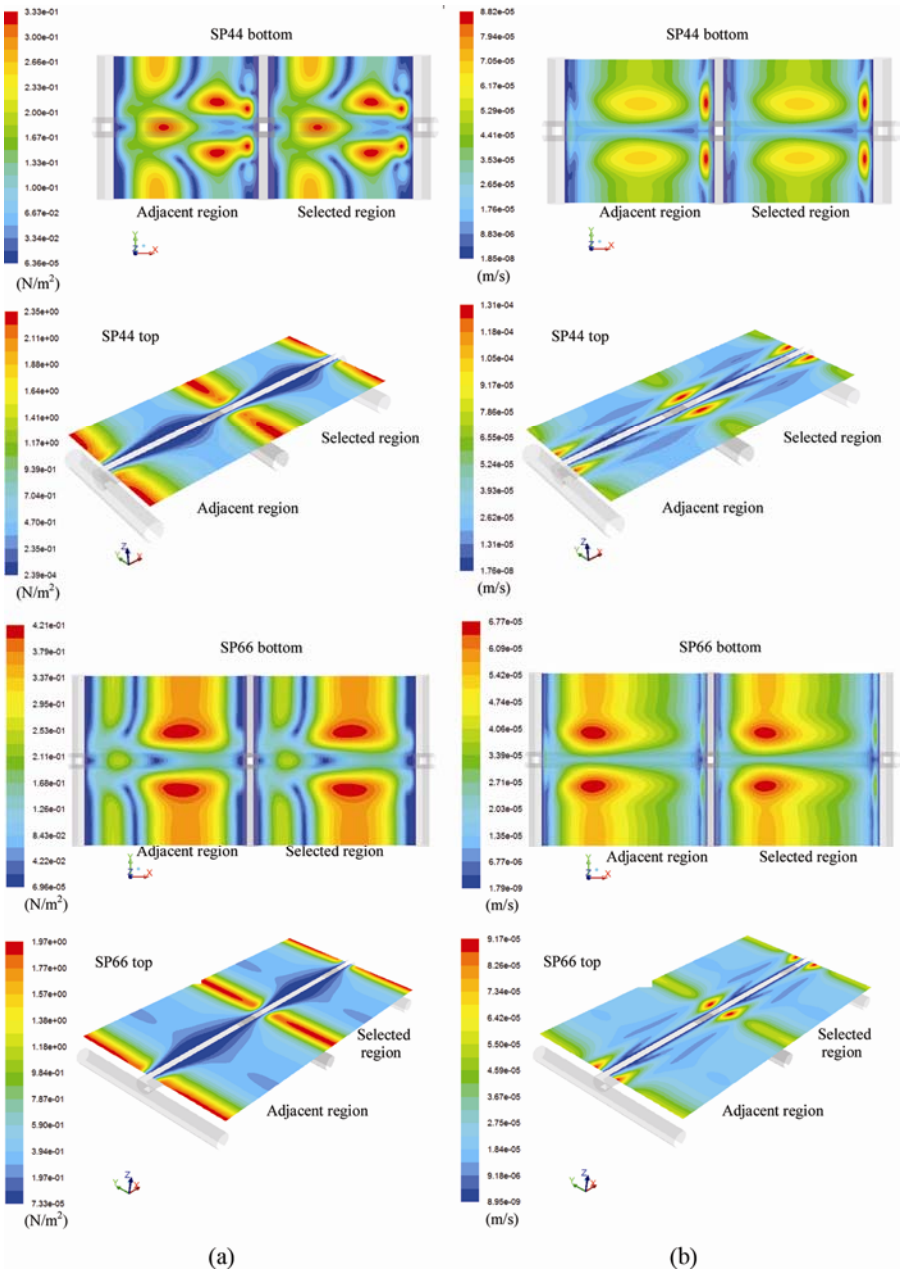

Figure 4 Velocity vectors coloured by velocity magnitude (fixed length) at a plane (a) close to top membrane (Z=0.95mm) & (b) close to bottom membrane (Z=0.05mm) for SP44 at Re_h=100.

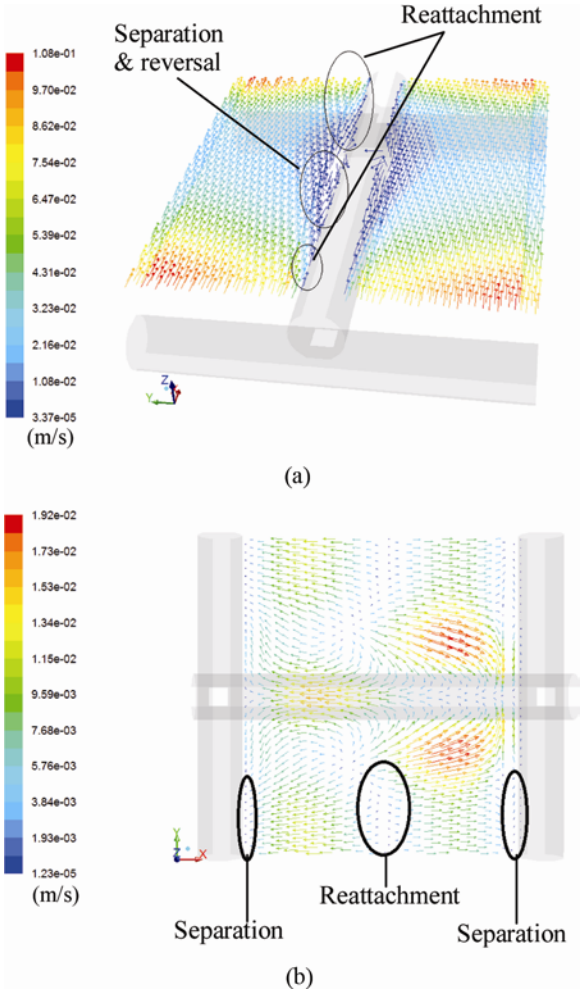

Figure 5 (a) Contours of velocity magnitude overlayed by the velocity vectors (fixed length) at vertical plane (y=0 mm) (b) bottom wall and (c) top wall shear stress and mass transfer coefficient distribution along flow direction at y=0mm, for SP44 at Re_h=100.

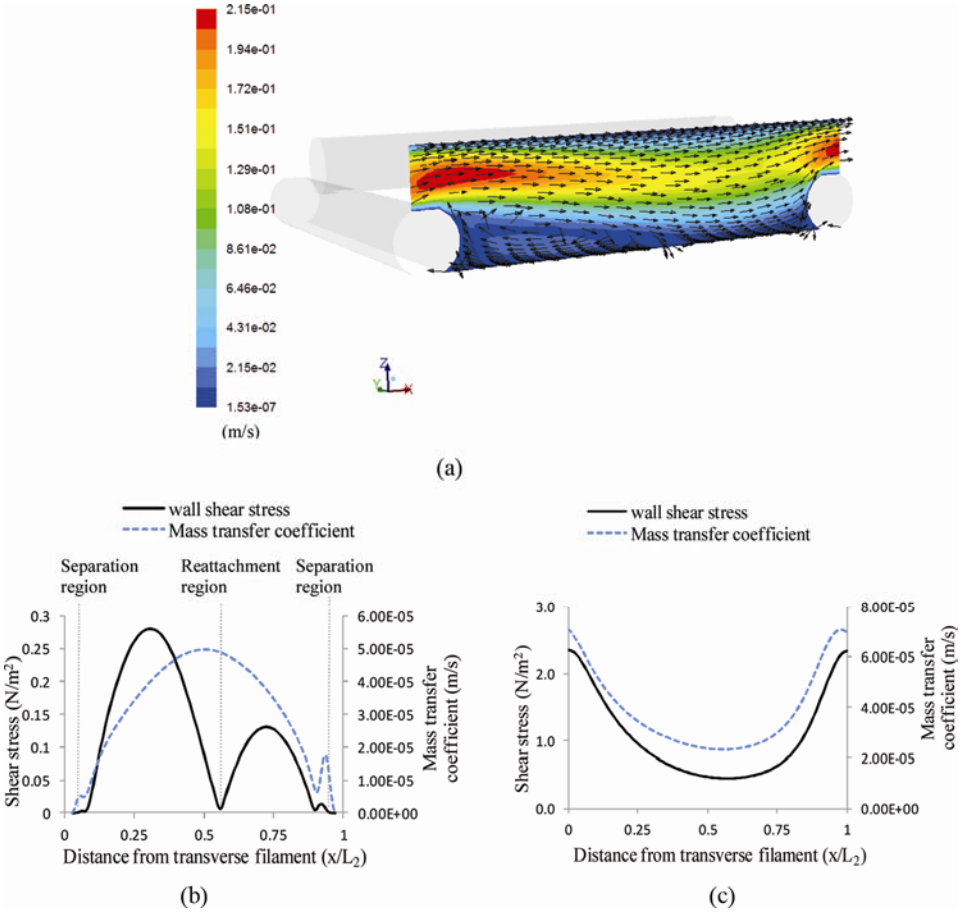

Figure 6 Velocity vectors (fixed length) overlayed by mass transfer coefficient at (a) top membrane surface (b) bottom membrane surface for different spacers at Re_h=100

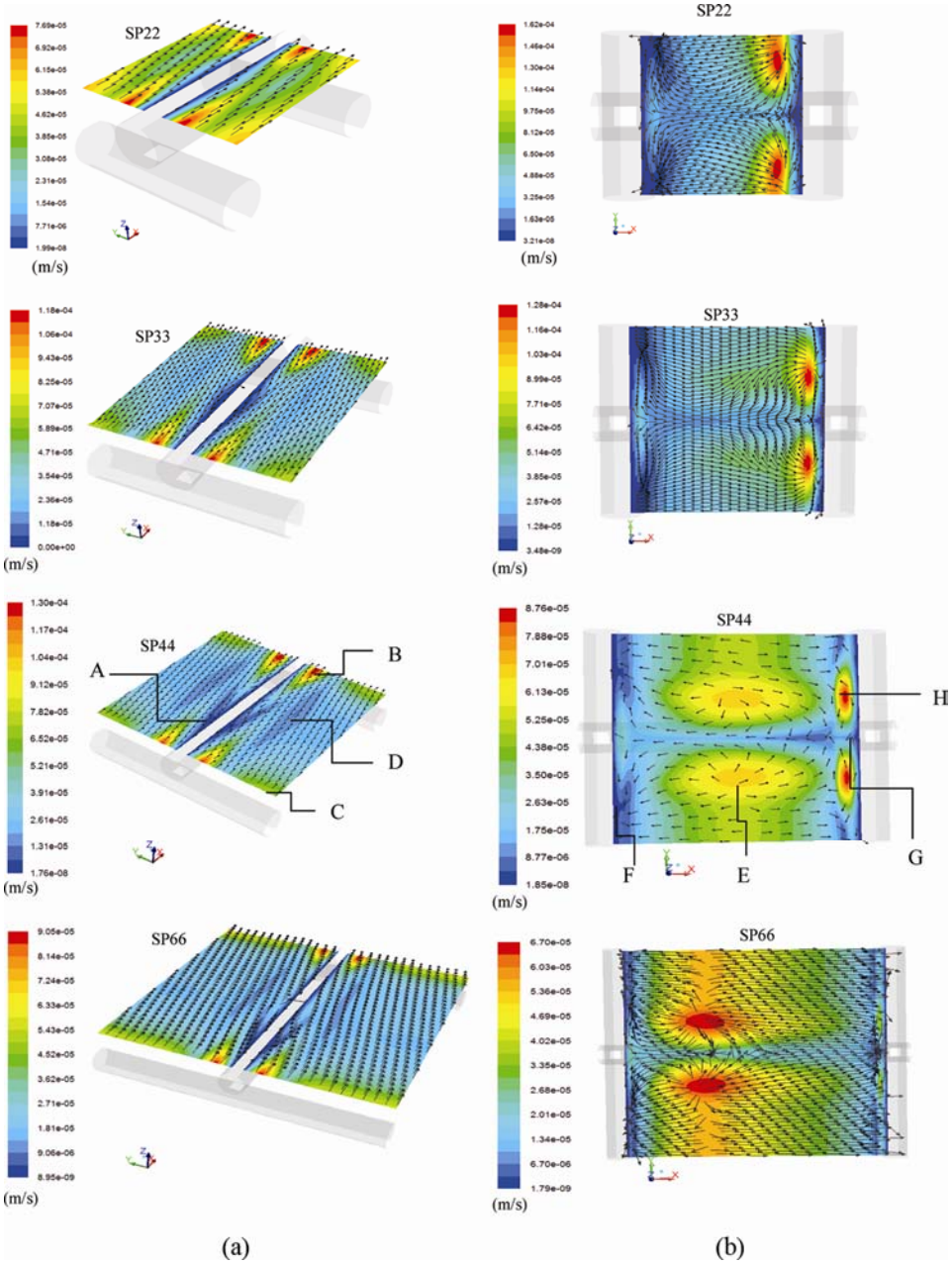

Figure 7 Average wall shear stress (a) and average mass transfer coefficient/pressure drop (b) against dimensionless filament spacing for different spacers at Reh=100.

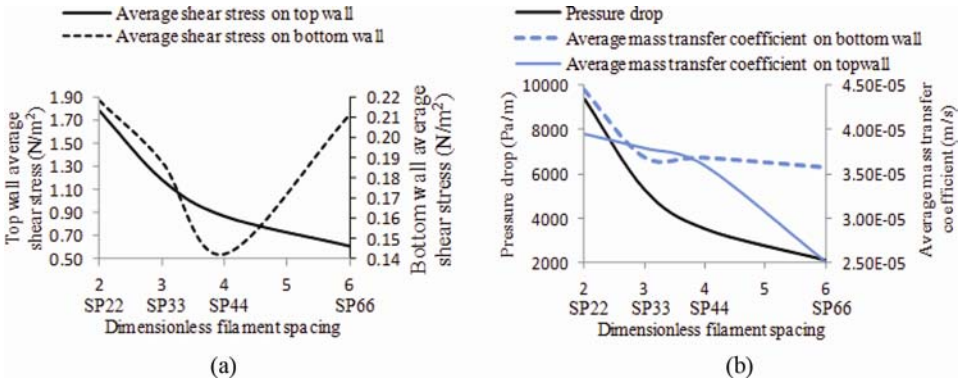

Figure 8 (a) Comparison of spacer configurations with experimental and numerical study of Geraldes et al. (Geraldes et al. 2002b) at Reh=100. (b): Comparison of Sherwood number for different spacer arrangement with previous studies (Da Costa et al. 1994; Li et al. 2004) at Sc=1350.

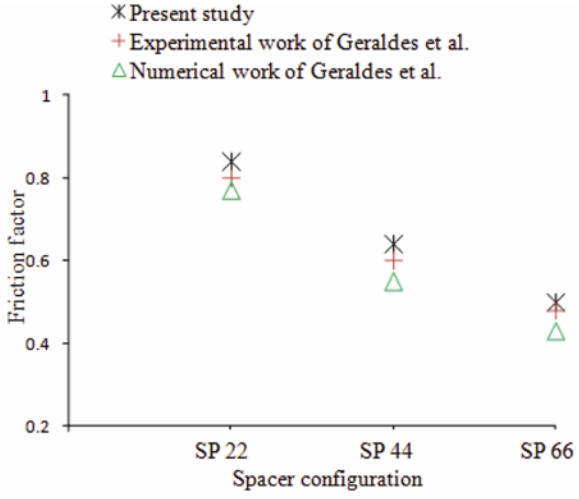

(a)

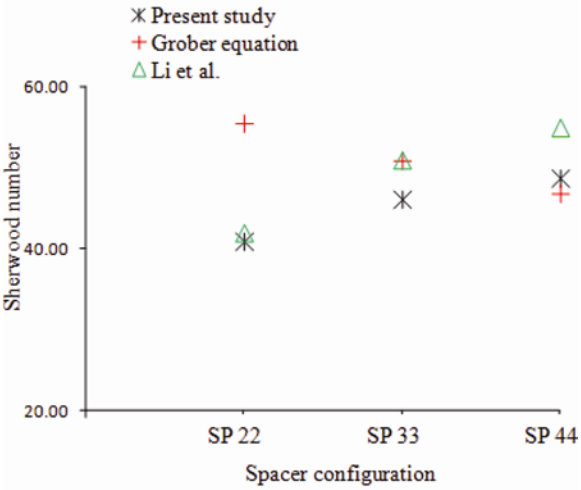

(b)